Ceramics International 50 (2024) 8586–8593

Contents lists available at ScienceDirect

Ceramics International

journal homepage: www.elsevier.com/locate/ceramint

Density and phase-purity of α-TCP obtained by sintering of nano-crystalline powder

Christoph Stähli [a,*], Antonio Jesus Salinas [b], Nicola Döbelin [a], Andrea Testino [c,d], Marc Bohner [a]

[a] RMS Foundation, Bischmattstrasse 12, 2544, Bettlach, Switzerland
[b] Universidad Complutense, Departamento de Química en Ciencias Farmacéuticas, Plaza de Ramón y Cajal, s/n, Ciudad Universitaria, 28040, Madrid, Spain
[c] Paul Scherrer Institut, Forschungsstrasse 111, 5232, Villigen PSI, Switzerland
[d] École Polytechnique Fédérale de Lausanne, STI SMX-GE, CH 1015, Lausanne, Switzerland

ARTICLE INFO

Handling Editor: Dr P. Vincenzini

Keywords:
Sintering (A)
Porosity (B)
Phase transition
Biomedical applications (E)

ABSTRACT

Dense and polished samples are sometimes used to test the *in vitro* biological response of biomaterials. However, their production can be challenging, for example for α-tricalcium phosphate (α-TCP), a commonly-used bone graft substitute. In this particular case, the ideal sintering conditions are in a temperature range close to the β-α-TCP phase transition (1125 °C). This phase transition is characterized by a 7 % volume increase which typically leads to the formation of cracks. Additionally, the production of a powder suitable for ceramic processing is difficult because α-TCP can only be produced via a thermal process. The initial aim of this study was to produce dense and polished α-TCP samples using an innovative method to produce nano-crystalline α-TCP. However, after observing the formation of β-TCP phase above the β-α-TCP phase transition (1125 °C), the focus of this study was shifted towards this unexpected phenomenon. Specifically, uniaxially compressed bulk samples were sintered at between 1160 and 1240 °C for different durations up to one week. The resulting density reached up to 95 % and was positively associated with green body density and sintering time, while being initially highest when sintered at the lowest temperature. A transient appearance of up to 6 wt% β-TCP was observed during sintering. The higher the sintering temperature was, the shorter and the smaller this transient appearance was. This behavior was attributed to the intrinsic pressure occurring within the material during sintering and which favoured the denser β-TCP phase.

1. Introduction

Calcium phosphate (CaP) ceramics have enjoyed widespread use as synthetic bone graft substitutes owing to their excellent biocompatibility, osteoconductivity, potential osteoinductivity and a chemical composition similar to bone mineral [1]. In particular, β-tricalcium phosphate (β-TCP, β-$Ca_3(PO_4)_2$) undergoes cell-mediated resorption *in vivo* at a rate matching the growth of new bone [2]. Its high-temperature polymorph α-TCP is more soluble, making it suitable as a constituent of *in situ*-setting bone cements. In addition, α-TCP has been used in products in the form of blocks and granules [3,4]. Given the different solubility and in turn biological properties of α- and β-TCP, control of the phase purity in the production of any TCP-based bioceramics is critical.

Dense and polished samples are sometimes used to test the *in vitro* biological response of biomaterials without interfering effects of the porosity or surface topography. For CaPs, dense samples allow for example to study osteoclastic resorption or chemical interactions between CaPs and aqueous solutions [5,6]. Dense bulk bioceramics with tailored microstructures have also been pursued with the aim to optimize their mechanical properties [7]. While hydroxyapatite (HA, $Ca_{10}(PO_4)_6O(OH)_2$) and β-TCP have been successfully prepared in a fully dense (and translucent) form [8,9], the highest densities reported for α-TCP are – to the best of our knowledge – approximately 95 % [10] and 97.3 % [11].

The production of dense and/or phase-pure α-TCP is challenging because α-TCP readily converts to β-TCP at temperatures slightly below the ideal sintering range of α-TCP. Two specific problems are encountered. First, the β- to α-TCP phase transformation, which occurs at 1125 °C, is accompanied by a 7 % volume expansion [12,13], thus resulting in mechanical stress which may induce cracks [14]. So, any phase change should be prevented. Second, sintering at temperatures significantly above the β- to α-TCP phase transition (1125 °C [3]) may

* Corresponding author.
E-mail address: christoph.staehli@rms-foundation.ch (C. Stähli).

https://doi.org/10.1016/j.ceramint.2023.07.068
Received 26 May 2023; Accepted 21 December 2023
Available online 8 July 2023

lead to excessive grain growth which hinders further densification [15]. Beside these two problems, there are additional difficulties. For example, given that small amounts of Sr or Mg – common impurities in CaPs – result in an increase of the β- to α-TCP phase transition temperature and in particular in the formation of a binary phase field of β- and α-TCP [16,17], the control of raw material purity is critical. Also, precursor quantities must be precisely adjusted in order to guarantee a molar Ca/P ratio of 1.50 and thus to avoid the presence of calcium pyrophosphate (CPP) or HA.

α-TCP powder produced by heat treatment above 1125 °C and subsequent milling commonly exhibits a particle size in the micro-meter range, which is not ideal for ceramic processing. In contrast, nano-powders (i.e. nano-sized primary particles or crystallites) exhibit a higher surface curvature and thus a higher reactivity towards thermally activated processes such as coarsening and sintering [18]. Therefore, green bodies formed from nano-powders are expected to allow for a high density upon sintering [19]. A previously described synthesis method of nano-crystalline α-TCP consists of the following two steps: i) a wet chemical precipitation of amorphous calcium phosphate (ACP), followed by ii) a short thermal treatment at 775 °C which results – according to Ostwald's step rule – in conversion to the kinetically favoured α-TCP phase and not the thermodynamically more stable β-TCP phase [20,21]. We have recently adopted this method and, in particular, optimized the critical drying steps of ACP after precipitation to consistently obtain phase- and chemically pure nano-crystalline α-TCP powder in suitable quantities for subsequent uniaxial pressing of bulk samples and sintering. In preliminary experiments, β-TCP was observed to form at the sintering temperature of 1200 °C, above the β- to α-TCP phase transition temperature [3].

The aim of this study was thus two-fold, namely i) to assess the potential of nano-crystalline α-TCP to produce dense bulk α-TCP, and ii) to explore the cause of the unexpected formation of β-TCP above the β- to α-TCP phase transition. For that purpose, the density, the phase composition and the microstructure were investigated as a function of green body density, sintering temperature and sintering time.

2. Materials and methods

2.1. Synthesis of nano-crystalline α-tricalcium phosphate

Nano-crystalline α-TCP was synthesized based on a previously described method [20,21]. In a first step, ACP was precipitated. Specifically, an ammonium phosphate solution (19.81 g $(NH_4)_2HPO_4$, puriss. p.a., Fluka, in 250 mL degassed and deionized water) was poured into a calcium nitrate solution (53.14 g $Ca(NO_3)_2{\cdot}4H_2O$, BioXtra, Sigma-Aldrich, in 250 mL water) previously mixed with ammonia for pH-adjustment (45 mL of 25 % aqueous ammonia solution, EMSURE®, Merck). The resulting precipitate was immediately stirred for 5 min and then subjected to a rigorous rinsing and drying procedure in order to maximize the phase-purity of the final α-TCP. Namely, the precipitated slurry was split into two halves which were each transferred onto a Buchner vacuum filter unit (cellulose filter papers, diam.: 12–15 μm, Carl Roth). The slurry was washed with a total of 4 L of 0.1 % aqueous ammonia solution (100 mL at a time on each filter unit), followed by 1 L of water and 200 mL of ethanol (99.8 %, Grogg Chemie) and subsequently resuspended in 300 mL ethanol, filtered once more and dried over night at room temperature. The powder was then sieved using a 0.5 mm sieve and dried by heating at a rate of 1 °C/min in a furnace (Nabertherm N20/14, with the flap open; split into powder heaps of ≤7 g) which was left to passively cool down as soon as the temperature reached 390 °C. Subsequently, the ACP was sieved again, converted into α-TCP in a preheated furnace at 775 °C for 20 min (Carbolite CDF 15/1B, with SiC heating elements; in powder heaps of ≤10 g) and then quenched at ambient air. Finally, the α-TCP powder was ball-milled for 2 h in isopropanol (≥99 %, Grogg Chemie) using zirconia milling balls and dried in a ventilated oven at 70 °C over night.

2.2. Pressing of sample pills

Aliquots of 200 mg of ball-milled α-TCP powder were pressed uniaxially into cylindrical pills of 6 mm diameter in a steel mould precoated with a 1 % stearic acid solution (puriss. p.a., Fluka) in ethanol. The mould was placed in a mechanical testing machine (Zwick 1475) in order to allow for a gradual and reproducible load cycle. Specifically, the load was increased at 4′000 N/min, kept at 4′000 N (140 MPa) for 1 min and released at 10′000 N/min. Alternatively, the load was increased at 10′000 or 20′000 N/min and kept at 10′000 or 20′000 N (350 or 710 MPa, respectively). The pills were then pushed out of the mould on a different testing machine (Zwick Z5.0), using a final speed of 0.1 mm/s with the goal to minimize fracturing resulting from internal stress. Nevertheless, a thin layer of the pills frequently chipped off the top surface of the cylinders upon expulsion from the mould and the specimens were therefore trimmed using a lathe to ensure a flat surface (final height between 3.3 and 4.0 mm).

2.3. Sintering

Three replicate pills per condition and a 40 or 200 mg aliquot of loose powder (control) were placed on a calcium stabilized zirconia tray (11.5 x 6 × 0.7 cm), inserted into a preheated furnace (Carbolite CDF 15/1B, with SiC heating elements) and kept at 1160, 1200 or 1240 °C for 0.5, 2, 6, 24, 72 or 168 h. The 95 % confidence interval (CI) of the temperature was ±15 °C, based on the annual furnace recalibration. Subsequently, the tray with the pills was taken out of the furnace, i.e. quenched at ambient air. Moreover, three replicate pills were quenched by dropping them into liquid N_2 within 15 s after taking them out of the furnace.

2.4. Characterisation methods

2.4.1. Trace element analysis

The elemental purity of nano-crystalline α-TCP was analysed using inductively coupled plasma-mass spectrometry (ICP-MS Agilent 7700x, Agilent Technologies). Powder aliquots were digested in 69 % HNO_3 and then diluted in a solution of demineralized H_2O containing 3 % HNO_3, 2 % HCl and 0.01 % HF (all: Rotipuran® Supra, Carl Roth). Signals of analyte elements were calibrated against certified multi- and single-element standard solutions (IV-ICPMS-71A, 71B and 71C, Hg and Bi, all: Inorganic Ventures). Signal drifts were corrected using an internal Sc and In standard solution measured along with each sample (Inorganic Ventures).

2.4.2. Specific surface area determination

The specific surface area (SSA) of the nano-crystalline α-TCP powder was determined (before ball-milling) via nitrogen adsorption using the Brunauer-Emmett-Teller (BET) method (Gemini 2360, Micromeritics). Specifically, measurements were done in triplicate and samples were dried at 130 °C for 2 h under nitrogen flow prior to the measurements.

2.4.3. Density measurements

Pressed green body and sintered cylinders were weighed and their dimensions measured using a calliper. The relative (apparent) density in %, d_r, was calculated as the ratio of the bulk density, d_b, to the theoretical density, d_{th}:

$$d_r = 100 \bullet \frac{d_b}{d_{th}} \tag{1}$$

with

$$d_b = \frac{m}{\pi(\varnothing/2)^2 \bullet h} \tag{2}$$

where m is the mass, ∅ the cylinder diameter (mean value of 2 mea-

surements in opposite directions), and h the cylinder height (mean value of 4 measurements at opposite positions), and

$$d_{th} = \frac{1}{\sum_i (f_i/d_i)} \quad (3)$$

where f_i are the relative weight fractions of each crystallographic phase (quantified by X-ray diffraction; XRD) and d_i are the corresponding theoretical phase densities ($d_{th,\alpha-TCP} = 2.86$ g/cm^3 [12], $d_{th,\beta-TCP} = 3.07$ g/cm^3 [13], $d_{th,\beta-CPP} = 3.13$ g/cm^3 [22], $d_{th,HA} = 3.15$ g/cm^3 [23]).

Consequently, the total porosity ratio in %, P, can be obtained as follows: $P = 100 - d_r$

2.4.4. Quantification of crystalline phases

XRD analysis was performed on sample pills and powders after sintering (as well as on ACP and α-TCP powder immediately after synthesis). Two fragments of each pill, or aliquots of powder, were finely ground in ethanol using a mortar and the resulting suspension was transferred onto single-crystal silicon sample holders and left to dry. Powder XRD patterns were collected using digitally and Ni-filtered CuKα radiation in reflection geometry from 4 to 60° 2θ at a step size of 0.012° and an acquisition time of 0.15 s per step. The resulting patterns were analysed by Rietveld refinement using Profex version 4.2.0-alpha [24]. The weight fractions of the following phases were quantified: α-TCP (PDF# 04-010-4348, [12]), β-TCP (PDF# 04-008-8714, [13]), β-CPP (PDF# 04-009-3876, [22]) and HA (PDF# 01-074-0565, [23]). For each condition (at sintering times >0 h), the mean value of the two pill fragments or powder aliquots was determined.

2.4.5. Scanning electron microscopy and energy-dispersive X-ray spectroscopy

Fragments of sintered pills were embedded in epoxy resin (Epofix resin and hardener, Struer) in a vacuum impregnation device (CitoVac, Struers) and polished using SiC paper (320- to 1200-grit), polishing paste (6 and 3 μm diamond particles, Struers) and finally a 0.2 μm fumed silica suspension (Akasel). The sections were then carbon-coated (sputter coater CCU-010, Safematic) and analysed by scanning electron microscopy (SEM) on a Zeiss Sigma 300 VP SEM at a working distance of approximately 8 mm and an acceleration tension of 15 kV using an energy-selective backscattered electron detector. An energy-dispersive X-ray (EDX) detector (Ultim® Max 40, Oxford Instruments) was used to quantify Ca and P contents in rectangular regions with an area in the order of 20–100 μm^2.

2.4.6. Thermogravimetric analysis (TGA), differential scanning calorimetry (DSC), evolved gas analyses (EGA) and thermomechanical analysis (TMA)

A pill pressed at 140 MPa were placed in alumina pans and analysed with a Mettler Toledo TGA/DSC in air (10 mL/min as reactive gas and 10 mL/min as protective gas). EGA were performed with a Pfeiffer Vacuum Thermostar (1–200 amu) mass spectrometer using a quartz capillary collecting the evolved gas above the sample pan and a transfer line heated at 150 °C. The pill was heated at 5 °C/min from 25 to 1100 °C and TGA/DSC/EGA signal collected.

The pill shrinkage upon heating was measured with a Setaram Setsys 1750 CS Evolution up to 1250 °C with a heating rate 5 °C/min in air (10 mL/min) using a hemispheric alumina probe and 2 g of load.

2.5. Statistical analysis

Statistical significance between data sets of density or β-TCP content as a function of sintering time and temperature was determined using two-way ANOVA followed by Bonferroni means comparison (Origin 2022, v9.9.0.225, OriginLab Corp.). Statistical significance between data sets of density or β-TCP content as a function of applied uniaxial pressure was determined using Student's t-tests.

3. Results

3.1. Characterization of nano-crystalline ACP and α-TCP powder

Fig. 1 presents XRD patterns of the precipitated and fully dried ACP, thus confirmed to be completely X-ray amorphous, and the α-TCP obtained following thermal treatment at 775 °C for 20 min. The phase purity of the latter was quantified by Rietveld refinement which revealed secondary phases of 1.8 ± 0.3 wt% β-TCP ($\chi^2 = 1.11$ [25]; n = 4) and β-CPP and HA contents below the detection limit (DL) for these phases (<0.5 wt%). The Ca/P ratio was very close to 1.50, as elaborated in section 3.3. The nano-structure of the α-TCP (Fig. 2) exhibited a similar morphology and characteristic size range as in an earlier study [20]. Nevertheless, in our material – in addition to rounded branches – some sheet-like structures as well as tiny needles with a thickness in the order of a few tens of nanometers were observed. The powder exhibited a specific surface area of 15.0 ± 0.6 m^2/g.

Screening for 63 metallic elements by ICP-MS revealed a high chemical purity, with the most abundant contaminant being Sr (224 mg/kg), followed by Mg (22 mg/kg), Zr (15 mg/kg; likely introduced during milling) and all other measured elements at contents below 10 mg/kg.

3.2. Apparent density of pressed pills before and after sintering

Sample pills were produced using different uniaxial pressures with the goal to modulate the resulting density. A higher uniaxial pressure led to a significantly higher relative (apparent) green body density (Fig. 3; blue symbols). This effect was still apparent, although not statistically significant, in the density after sintering for 6 h at 1200 °C (Fig. 3; orange symbols). Specifically, by applying a pressure of 710 MPa, a 96.1 % dense pill (i.e. containing 3.9 % porosity) was obtained. However, higher pressures frequently resulted in breaking of sample pills upon expelling from the mould. Therefore, for the continuation of the study – focussing on the effect of sintering time and temperature – pills were pressed using a uniaxial pressure of 140 MPa.

The relative density of sample pills after sintering for various times at different temperatures is shown in Fig. 4. The relative density of the same pills before sintering is shown in the grey inlay (sintering time '0 h'; classed per the three respective temperatures at which they were subsequently sintered), confirming the consistency of the green body samples. Sintering for only 0.5 h already resulted in a high densification, with the highest density obtained at the lowest sintering temperature of 1160 °C. Sintering at this temperature for longer durations did not lead to significantly higher densities. Sintering at 1200 and 1240 °C resulted in a gradually increasing density over time which – after approximately 24 h – reached values similar to the density obtained when sintering at 1160 °C. The highest density achieved was 94.7 % by sintering for 168 h

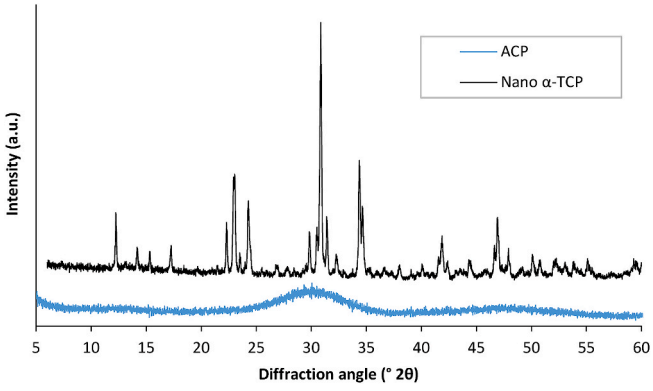

Fig. 1. XRD patterns of nano-crystalline ACP and α-TCP after thermal treatment at 775 °C for 20 min (The α-TCP pattern was shifted vertically for better representation).

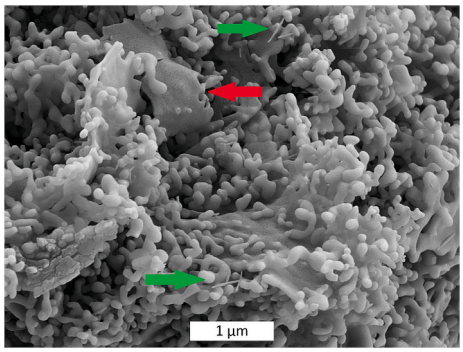

Fig. 2. SEM image of non-sintered nano-α-TCP powder. Arrows indicate sheet-like structures (red) and needles (green).

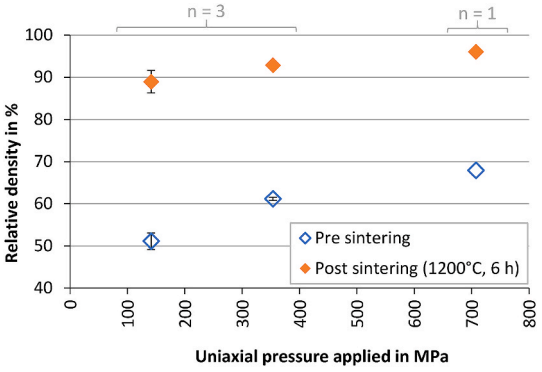

Fig. 3. The effect of the pressure applied for green body production on the relative density before and after sintering for 6 h at 1200 °C (±15 °C; 95 % CI). Error bars designate the standard deviation (SD) over the three replicate pills at 140 and 350 MPa (only one pill was available at 710 MPa). The density both before and after sintering increased with pressure. Between 140 and 350 MPa, the difference was statistically significant before but not after sintering ($p < 0.01$).

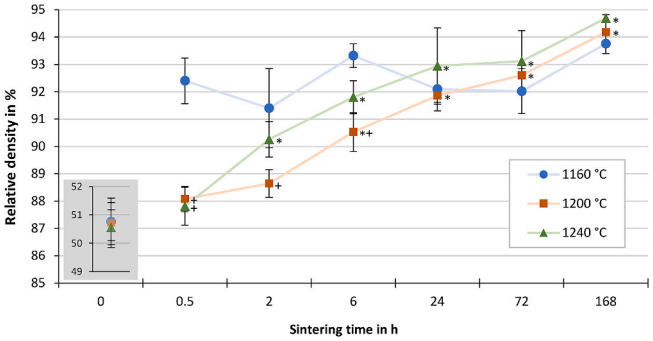

Fig. 4. The relative density of pills pressed at 140 MPa as a function of sintering time and temperature (±15 °C; 95 % CI). Grey inlay: before sintering. Error bars designate the SD over the three replicate pills per condition. Statistical significance ($p < 0.05$) is indicated for each sintering time vs. the shortest sintering time (0.5 h) at a given temperature (*) and for each temperature vs. the lowest temperature (1160 °C) at a given time (+). At 1160 °C, the density did not change significantly over time. At 1200 and 1240 °C, the density was initially significantly lower compared to 1160 °C, but increased over time to reach the range of density determined in pills sintered at 1160 °C.

at 1240 °C. Note that the effect of temperature at that sintering time was not statistically significant (means comparisons at 168 h, $p < 0.05$). Nevertheless, considering all data over all sintering times, the mean values between all three sintering temperatures were significantly different (overall means comparisons, $p < 0.05$).

With the goal to better understand the observed dependency of the density on sintering parameters, temperature-resolved analyses with a heating rate of 5 °C/min were performed (TMA and TGA/DSC/EGA). TMA analysis showed swelling between approximately 1150 and 1200 °C (Suppl. Fig. 1) which was in agreement with the densities measured after 0.5 h of sintering (Fig. 4). Specifically, the maximum relative density determined by TMA, 94.3 %, was achieved at 1150 °C, whereas at 1180 °C, the relative density decreased to 89.4 % and further decreased to 88.8 % at 1250 °C.

TGA/EGA showed an initial release of water up to 160 °C, which corresponds to ≈0.5 wt% and other two minor water loss contributions at around 200 and 320 °C, the latter combined with CO_2 release too (Suppl. Fig. 2 to Suppl. Fig. 4). Overall, 1.2 % weight loss was measured, which coincides with a consistent weight loss of ≈1.3 % observed in pills before and after sintering. TMA combined with TGA/EGA also showed an additional feature at ≈ 800 °C, associated to CO_2 release (Suppl. Fig. 4), which might be an ascribed thermal decomposition of a minor amount of carbonate (weight loss ≈ 0.1 %, Suppl. Fig. 2) and a DSC signal that indicates an endothermic and then an exothermic reaction (Suppl. Fig. 5). These reactions coincided with a ≈5 % increase of the relative the density (Suppl. Fig. 1).

3.3. Phase composition of pressed pills and powder after sintering

In order to assess the phase purity of the α-TCP pills during sintering, XRD measurements were performed on crushed pills as well as powder aliquots after sintering for various times at different temperatures. An example of the Rietveld refinement in the case of a pill sintered for 72 h at 1160 °C is presented in Fig. 5. Refinement statistics and the unit-cell parameters obtained from the Rietveld refinement are provided in Table 1. The β-TCP content for all sintering conditions and both sample types is shown in Fig. 6. At all sintering temperatures, a transient formation of β-TCP was observed despite these temperatures being in the stability region of α-TCP, i.e. significantly above 1125 °C [3], even when taking into account the uncertainty on the furnace temperature. The lower the sintering temperature (i.e. the closer to the α- to β-TCP transformation temperature), the more strongly the β-TCP content increased and the later the maximum occurred. At sintering temperatures 1200 and 1240 °C, β-TCP was almost entirely eliminated after 168 and 72 h, respectively. In contrast to sample pills, the β-TCP content of powder aliquots decreased from the initial value within only 0.5 h of sintering and – except at 1160 °C – remained very close to or below the DL for β-TCP of the refinement method (0.4 wt%). Note that in the case of 24 h and 1160 °C, a powder heap with the same weight as a pill was prepared (200 mg; thus occupying a higher volume than a pill) in order to exclude a faster cooling rate in the powder than in pills. Still, the β-TCP content was significantly lower than that of the pills, even in an aliquot taken from the center of this powder heap. The β-CPP and HA contents in pills as well as powders remained below or only slightly above the DL for these phases (0.5 wt%) throughout the sintering study. Specifically, the highest mean β-CPP and HA contents quantified in any sintering condition were 0.8 and 0.6 wt%, respectively. Consequently, the Ca/P ratio was 1.497 ± 0.001 (mean and standard deviation over 20 sintering conditions; considering also β-CPP and HA signals below the DL). Assuming that no or negligible phosphate evaporation occurred during sintering [26], this Ca/P ratio also pertains to the raw powder. Note that the EGA did not identify any signal attributable to P gaseous species up to 1100 °C in the range 0–200 *m/z*.

In order to exclude an artifact resulting from cooling of the pills through the β-TCP temperature region at the end of each time point, pills were also quenched in liquid N_2 in parallel to pills quenched at ambient air (after sintering for 72 h at 1160 °C). The β-TCP content was not significantly different ($p > 0.05$) between the two methods (Suppl. Fig. 6), thus confirming that β-TCP was indeed formed during sintering.

The uniaxial pressure applied during pill production did not have a

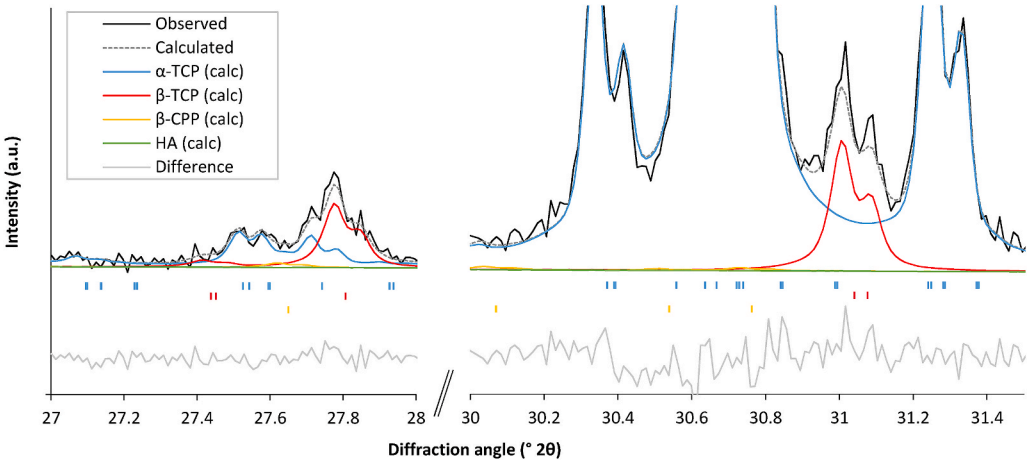

Fig. 5. Result of the Rietveld refinement (in two areas of interest for β-TCP quantification) of the XRD pattern of a pill pressed at 140 MPa and sintered for 72 h at 1160 °C. Observed and calculated (fitted) signals – the latter representing the sum of the four phase models included in the refinement – as well as the difference between the two are shown. Furthermore, Bragg positions (tick marks) are indicated. Two β-TCP peaks at 27.8 and 31.0 °2θ exhibited only little overlap with the α-TCP signal and thus allowed for robust quantification of the β-TCP phase fraction (here: 6.0 wt%).

Table 1
Refinement statistics and refined unit-cell parameters. Mean and standard deviations over at least 126 data sets (obtained on sintered pills or powder samples) are provided.

Refinement statistics	
χ^2 (defined in Ref. [25])	1.23 ± 0.11 (n = 140)
Unit cell α-TCP (space group P12_1/a1; PDF# 04-010-4348, [12]*)*	
a (Å)	12.881 ± 0.004 (n = 140)
b (Å)	27.290 ± 0.012 (n = 140)
c (Å)	15.221 ± 0.001 (n = 140)
β (°)	126.20 ± 0.02 (n = 140)
Unit cell β-TCP (space group R3c; PDF# 04-008-8714, [13]*)*	
a (Å)	10.433 ± 0.009 (n = 126)
c (Å)	37.425 ± 0.058 (n = 126)

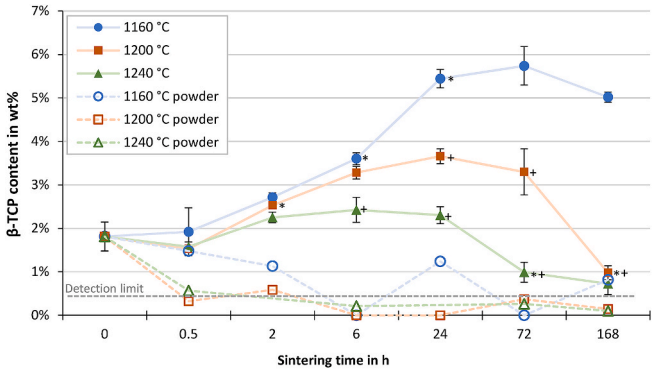

Fig. 6. The β-TCP content of pills pressed at 140 MPa as well as powders as a function of sintering time and temperature (±15 °C; 95 % CI). Error bars designate the SD over the three replicate pills per condition, or four powder aliquots at sintering time 0 h. Statistical significance ($p < 0.05$) is indicated (for pills only) for each sintering time vs. the next shorter time at a given temperature (*) and for each temperature vs. the next lower temperature at a given time (+). The grey dashed line designates the detection limit (DL), defined as 2.77 x the estimated SD calculated by the refinement algorithm. At all temperatures, the β-TCP content in pills exhibited an initial increase followed by a decrease over time. Lower sintering temperatures resulted in a higher and later-occurring maximum β-TCP content. Powder aliquots sintered in parallel with the pressed pills contained no or very little β-TCP (mainly at 1160 °C).

significant effect on the β-TCP content after sintering for 6 h at 1200 °C (see Suppl. Fig. 7). Note that the β-TCP content reported in Suppl. Fig. 7 (at an applied pressure of 140 MPa) is slightly higher compared to the equivalent sintering conditions in Fig. 6 because a different nano-α-TCP batch was used.

The height of the green body pills varied slightly (mean ± SD: 3.70 ± 0.14 mm; n = 54) due to a necessary trimming step after pressing (see section 2.2). In order to exclude artifacts arising from the pill height in the study of the effect of sintering time and temperature, pills were assigned to each condition (sintering time/temperature) by ensuring a very similar mean pill height per condition. Nevertheless, a potential effect of pill height on the β-TCP content was assessed but was not statistically significant ($p > 0.05$; detailed in Suppl. Fig. 8).

3.4. Microstructure of sintered pills

SEM images of polished cross sections of pills sintered for various times at different temperatures are shown in Fig. 7 (and at lower magnification in Suppl. Fig. 9). Round pores with diameters partly below 1 μm are apparent in all samples. For short sintering times, pores were rather homogeneously distributed, whereas after longer sintering, pore-free and pore-rich zones developed. Moreover, after 168 h of sintering, some larger pores with diameters in the order of or greater than 5 μm can be seen. This process was slightly more distinct – or occurred more rapidly – at higher sintering temperatures. The microstructure after 0.5 h of sintering at 1160 °C exhibited a large number of cracks, which was confirmed in two separate pills (observable especially in Suppl. Fig. 9).

Areas distinctly brighter than the surrounding zone, i.e. indicating a denser material in the backscattered electron mode, were observed in all pills regardless of sintering time and temperature. These brighter areas contained no or only very few pores. (A high magnification image of a dense zone is shown in Suppl. Fig. 10). EDX analysis revealed a significantly ($p < 0.001$) lower Ca/P molar ratio in bright areas (1.52 ± 0.02, n = 12 sample regions) compared to surrounding zones (1.57 ± 0.01, n = 12 sample regions). Note that i) lowering the acceleration voltage in order to minimize the interaction volume did not affect the Ca/P ratio and ii) the absolute Ca/P values cannot be guaranteed because systematic errors of the EDX method are unknown.

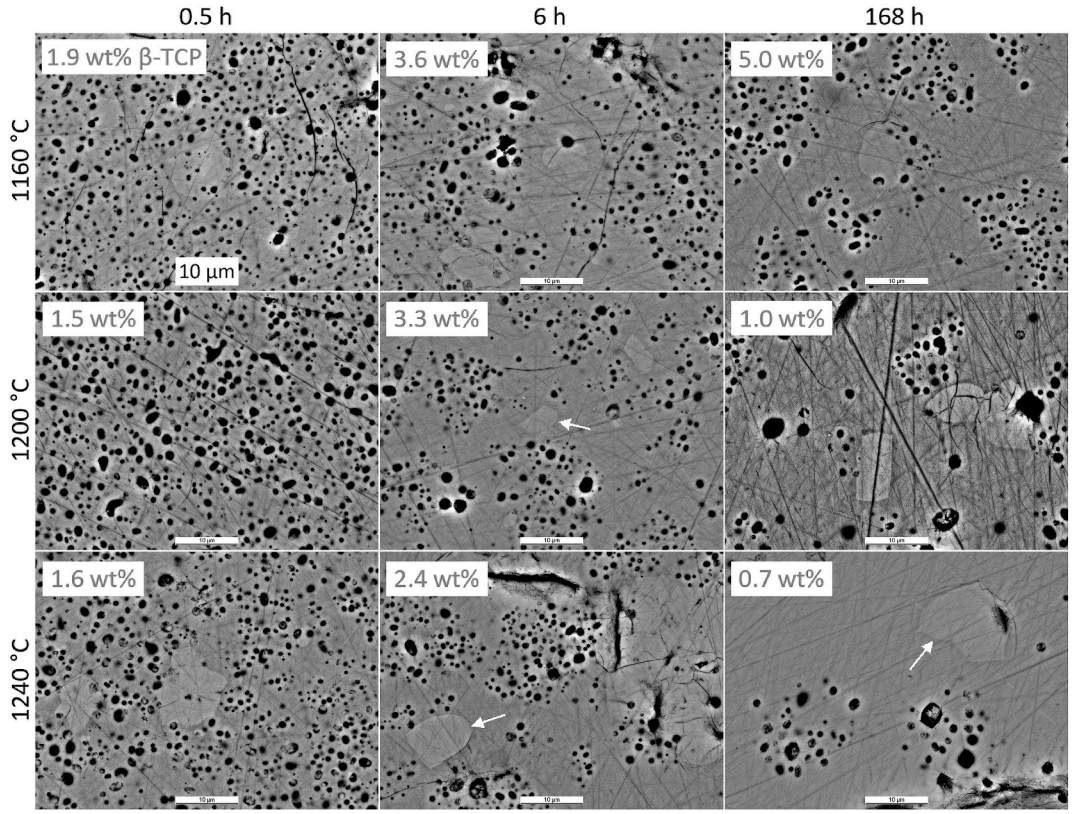

Fig. 7. SEM images acquired using a backscattered electron detector of polished cross sections of pills sintered for different times and at different temperatures (±15 °C; 95 % CI). Scale bar: 10 µm. Grey: β-TCP phase fraction as described in section 3.3. Over time, pores agglomerated into clusters and eventually merge into larger pores. Distinct bright areas can be seen in all samples (white arrows – also shown at higher magnification in Suppl. Fig. 10). Overview images obtained at lower magnification of the same pills are shown in Suppl. Fig. 9.

4. Discussion

In this study, a previously reported synthesis method of nano-crystalline α-TCP via ACP precipitation was adopted [20,21]. The washing and drying of the ACP are critical to ensure a precise Ca/P ratio and ultimately a phase pure α-TCP. In particular, insufficient drying but also drying at too high temperatures result in crystallization of calcium-deficient hydroxyapatite (CDHA; $Ca_9(PO_4)_5(HPO_4)OH$) which is known to be transformed to β-TCP instead of α-TCP during the thermal treatment at 775 °C [27]. We have optimized the drying procedure and found that the highest purity is achieved by slow heating up to 390 °C, while upscaling must be done under consideration of the diffusion distances of released moisture, i.e. the size of powder heaps. As a result, we have obtained α-TCP with a precise Ca/P ratio and no detectable β-CPP or HA. The presence of 1.8 wt% β-TCP suggests that the ACP may have contained traces of CDHA (despite being fully XRD-amorphous), or that the optimal duration of the thermal treatment is slightly less than 20 min. Nevertheless, phase pure α-TCP can be obtained after sintering as shown in this study. Moreover, a high chemical purity was obtained owing to careful choice of raw materials.

Nano-crystalline α-TCP offers a promising starting material to produce dense α-TCP for its application in investigations of materials properties where artifact effects of microstructure and porosity are undesirable. Yet, the highest density achieved here (94.7 %) was in the same range or slightly lower than previously reported values. Specifically, a density of approximately 95 % [10] and 97.3 % (porosity: 2.7 %; after two-step sintering [11]) have been reported, although the latter study provided only little information on the statistical significance and reproducibility of the data. We have applied the same two-step sintering profile – with temperatures of 1400 and 1300 °C, respectively [11] – to our nano-crystalline α-TCP but obtained only a density of 93.7 ± 0.6 % (mean ± SD, n = 3). Unsurprisingly, our materials were not translucent, in contrast to some reports of dense HA and β-TCP [8,9]. Nevertheless, our findings elucidate the effects of green body density and sintering parameters on the resulting density and microstructure (as well as on the phase composition). Specifically, the results of this study demonstrate that to maximize the density, a uniaxial pressure must be chosen by weighing the advantage of a high green body density against the challenge of cracking upon demoulding. Longer sintering times generally led to higher densities (Fig. 4), suggesting that sintering for several weeks may offer one approach to reach densities close to 100 %. The role of the temperature was complex with a lower density after 0.5 h of sintering at 1200 or 1240 °C compared to 1160 °C. This difference appears to be a result of swelling while the temperature rises from 1150 to 1200 °C, as observed by TMA (Suppl. Fig. 1). However, the transitions shown by TMA – both at ≈ 800 and 1150 °C – may also be due to a temporary phase transformation to β-TCP during heating. Note that such a phase transformation does not pertain to the results shown in Fig. 4 where samples consisted of almost pure α-TCP after 0.5 h of sintering (Fig. 6). (The different heating rates between TMA and the sintering study must be considered when comparing these findings). Furthermore, the features observed by TGA/DSC/EGA close to 800 °C (Suppl. Fig. 2 to Suppl. Fig. 5) match a previous report of carbonate volatilisation during heating of ACP [28]. Further investigation is needed to understand the cause of these phenomena.

The pores appeared more rounded and generally smaller than what is commonly observed in sintered CaP ceramics (Fig. 7). This feature points towards pores being intra-rather than inter-granular [18], resulting from fast grain boundary movement during sintering. The gradual reduction of the number of pores and merging into larger pores is consistent with the classical driving force of surface area reduction. In intra-granular pores, this process is known to be slow since it is

dependent exclusively on bulk vacancy diffusion [18], which agrees with the observations in this study, namely only a very limited progress in densification over one week of sintering. The fast grain growth presumed here suggests that the applied sintering temperatures were higher than ideal. However, lowering the sintering temperature is impeded by the β- to α-TCP phase transition (1125 °C) which thus underlines that densification of α-TCP is more challenging than for other CaP phases, as elaborated in the introduction (section 1).

The transient formation of β-TCP at temperatures in the stability region of α-TCP (Fig. 6) represents an unexpected complication in the quest to obtain dense and pure α-TCP, but also a discovery that has – to the best of our knowledge – never been reported so far. We propose the hypothesis that compressive forces in the microstructure during sintering favoured the 7 % denser β-TCP phase [12,13]. Indeed, there was no increase in the β-TCP content over time in powder aliquots sintered in parallel with pressed pills. The sintering pressure has been described in different models as being proportional to the surface energy and the curvature of a pore surface [29,30]. Thus, the small closed pores observed here plausibly generate a relatively high pressure in the body.

It is known from materials other than CaPs that pressure favours crystallographically denser phases. For example, the p-T-diagram of SiO_2 states that the transition temperature of α- to β-quartz (2.65 and 2.48 g/cm^3, respectively) or of coesite (2.91 g/cm^3) to α-quartz increases with pressure [31,32]. Equivalently, the transition temperature of monoclinic (5.68 g/cm^3) to tetragonal zirconia (6.10 g/cm^3) decreases with pressure [33,34]. Hence, an intrinsic pressure would lead to an increase of the β- to α-TCP transition temperature. While no quantitative thermodynamic or kinetic models are provided in this study, we hypothesize that the phase transition temperature rose to slightly above 1240 °C, thus causing a driving force for β-TCP formation that is proportional to the difference between the transition temperature and the applied temperature, in line with the observation that more β-TCP was formed at lower temperatures. The fact that the β-TCP content decreased again from its maximum after several days of sintering suggests that the pressure returned to atmospheric level, in line with gradually coalescing pores and hence a decrease of the curvature. Consequently, the phase transition temperature would have reverted to 1125 °C. Future work involving sintering under non-atmospheric pressure may help corroborate this explanation.

Alternative causes for the transient formation of β-TCP were considered but did not provide a satisfactory explanation as discussed in the following. i) Temperature gradients may have occurred within the furnace shortly after inserting the samples. However, beyond a few minutes, i.e. over the time periods investigated in these experiments, no more transient temperatures were recorded in the furnace. ii) After removing the samples from the furnace, their temperature passed through the stability region of β-TCP. However, quenching in air was shown to be sufficiently rapid since it resulted in the same final β-TCP content as quenching in liquid N_2. Note that approximately 15 s passed between opening the furnace and dropping the pills into liquid N_2 which is much shorter than the time frames required for the α- to β-TCP phase transition [35]. Moreover, β-TCP appeared only at specific time points and temperatures in our study – and not in powders – although quenching was performed identically in all experiments. iii) Finally, impurity elements such as Mg or Sr affect the β- to α-TCP phase transition temperature [16,17]. However, the reported increase in the transition temperature (and the presence of a binary phase field) occurred at several percent of Mg or Sr, while the α-TCP used in this study contained only 22 mg/kg Mg and 224 mg/kg Sr. In addition, impurity elements would affect the equilibrium state of the phase composition and cannot explain a transient formation of β-TCP.

The spatial distribution of the β-TCP phase in the microstructure could not be revealed in this study. Although distinct brighter zones were observed in backscatter SEM images, which would suggest a denser phase like β-TCP, these zones were present after all sintering times and temperatures and hence do not correlate with the phase composition results. The brighter zones seen in some of the SEM images exhibited a Ca/P ratio slightly lower than 1.50 as revealed by EDX analysis, suggesting the presence of β-CPP grains (Ca/P = 1.0; density = 3.13 g/cm^3 [22]). However, the exact elemental quantification may have been affected by an artifact effect resulting from the higher density (such as in β-TCP or other phases). Future work including EBSD is necessary to clarify the phase distribution both in and outside the bright appearing zones.

5. Conclusions

Sintering of nano-crystalline, uniaxially compressed α-TCP resulted in up to 95 % dense α-TCP, along with a transient appearance of up to 6 wt% β-TCP. While not having produced a higher α-TCP density than previously reported, the findings obtained in this study are expected to contribute to future improvements of the density, owing to a better understanding of the role of green body density as well as an optimized thermal profile. The unexpected transient phase composition, which contradicts the commonly accepted phase diagram for atmospheric pressure, appears to be the result of an intrinsic pressure in the microstructure. The discovery of this phenomenon may help manufacturers ensure the phase-purity of TCP bone substitute materials.

Declaration of competing interest

The authors declare that they have no known competing financial interests or personal relationships that could have appeared to influence the work reported in this paper.

Acknowledgements

This project was internally funded by RMS Foundation. A.J. Salinas was funded by Instituto de Salud Carlos III [project number PI20/01384]. The authors would like to thank Pascal Michel, Yves Viecelli, Francesco Pavan, Stefan Röthlisberger and Fabrizio Bigolin for their valuable help in this work.

Appendix A. Supplementary data

Supplementary data to this article can be found online at https://doi.org/10.1016/j.ceramint.2023.07.068.

References

[1] R.Z. LeGeros, Properties of osteoconductive biomaterials: calcium phosphates, Clin. Orthop. Relat. Res. 395 (2002) 81–98. http://www.ncbi.nlm.nih.gov/entrez/query.fcgi?cmd=Retrieve&db=PubMed&dopt=Citation&list_uids=11937868.

[2] M. Bohner, B.L.G. Santoni, N. Döbelin, β-tricalcium phosphate for bone substitution: synthesis and properties, Acta Biomater. 113 (2020) 23–41, https://doi.org/10.1016/j.actbio.2020.06.022.

[3] R.G. Carrodeguas, S. De Aza, α-Tricalcium phosphate: synthesis, properties and biomedical applications, Acta Biomater. 7 (2011) 3536–3546, https://doi.org/10.1016/j.actbio.2011.06.019.

[4] S. V Dorozhkin, Calcium orthophosphates as bioceramics: state of the art, J. Funct. Biomater. 1 (2010) 22–107.

[5] S.A. Redey, S. Razzouk, C. Rey, D. Bernache-Assollant, G. Leroy, M. Nardin, G. Cournot, Osteoclast adhesion and activity on synthetic hydroxyapatite, carbonated hydroxyapatite, and natural calcium carbonate: relationship to surface energies, J. Biomed. Mater. Res. 45 (1999) 140–147. http://www.ncbi.nlm.nih.gov/entrez/query.fcgi?cmd=Retrieve&db=PubMed&dopt=Citation&list_uids=10397968.

[6] B. Le Gars Santoni, L. Niggli, S. Dolder, O. Loeffel, G.A. Sblendorio, R. Heuberger, Y. Maazouz, C. Stähli, N. Döbelin, P. Bowen, W. Hofstetter, M. Bohner, Effect of minor amounts of β-calcium pyrophosphate and hydroxyapatite on the physico-chemical properties and osteoclastic resorption of β-tricalcium phosphate cylinders, Bioact. Mater. 10 (2022) 222–235, https://doi.org/10.1016/j.bioactmat.2021.09.003.

[7] M. Eriksson, Y. Liu, J.F. Hu, L. Gao, M. Nygren, Z.J. Shen, Transparent hydroxyapatite ceramics with nanograin structure prepared by high pressure spark plasma sintering at the minimized sintering temperature, J. Eur. Ceram. Soc. 31 (2011) 1533–1540, https://doi.org/10.1016/j.jeurceramsoc.2011.03.021.

[8] M. Jarcho, R.L. Salsbury, M.B. Thomas, R.H. Doremus, Synthesis and fabrication of b-tricalcium phosphate (whitlockite) ceramics for potential prosthetic applications, J. Mater. Sci. 14 (1979) 142–150, https://doi.org/10.1007/BF01028337.
[9] E. Champion, Sintering of calcium phosphate bioceramics, Acta Biomater. 9 (2013) 5855–5875, https://doi.org/10.1016/j.actbio.2012.11.029.
[10] C. Ohtsuki, K. Yamaguchi, T. Uchino, G. Kawachi, K. Kikuta, M. Kamitakahara, Formation of bone-like apatite on tricalcium phosphate ceramics in a solution mimicking body fluid, Adv. Bioceram. POROUS Ceram. 29 (2009) 189–198.
[11] I.Y. Kim, J. Wen, C. Ohtsuki, Fabrication of α-tricalcium phosphate ceramics through two-step sintering, Key Eng. Mater. 631 (2015) 78–82. https://doi.org/10.4028/www.scientific.net/KEM.631.78.
[12] M. Mathew, L.W. Schroeder, B. Dickens, W.E. Brown, The crystal structure of a-Ca3 (PO4)2, Acta Crystallogr. B33 (1977) 1325–1333.
[13] B. Dickens, L.W. Schroeder, W.E. Brown, Crystallographic studies on the role of Mg as a stabilizing impurity in b-Ca3(PO4)2 I. The crystal structure of pure b-Ca3 (PO4)2, J. Solid State Chem. 10 (1974) 232–248.
[14] H.S. Ryu, H.J. Youn, K.S. Hong, B.S. Chang, C.K. Lee, S.S. Chung, An improvement in sintering property of beta-tricalcium phosphate by addition of calcium pyrophosphate, Biomaterials 23 (2002) 909–914. http://www.ncbi.nlm.nih.gov/entrez/query.fcgi?cmd=Retrieve&db=PubMed&dopt=Citation&list_uids=11771710.
[15] A. Indurkar, R. Choudhary, K. Rubenis, J. Locs, Advances in sintering techniques for calcium phosphates ceramics, Mater 14 (2021) 6133, https://doi.org/10.3390/ma14206133.
[16] R.G. Carrodeguas, A.H. De Aza, X. Turrillas, P. Pena, S. De Aza, New approach to the beta-alpha polymorphic transformation in magnesium-substituted tricalcium phosphate and its practical implications, J. Am. Ceram. Soc. 91 (2008) 1281–1286. http://www.scopus.com/scopus/inward/record.url?eid=2-s2.0-41549162406&partnerID=40&rel=R8.0.0.
[17] J.F. Sarver, M. V Hoffman, F.A. Hummel, Phase equilibria and tin-activated luminescence in strontium orthophosphate systems, J. Electrochem. Sco. 108 (1961) 1103–1110.
[18] M.N. Rahaman, Ceramic Processing and Sintering, second ed., CRC Press, Boca Raton, 2003. https://doi-org.bib-ezproxy.epfl.ch/10.1201/9781315274126.
[19] J. Li, H. Liao, L. Hermansson, Sintering of partially-stabilized zirconia and partially-stabilized zirconia-hydroxyapatite composites by hot isostatic pressing and pressureless sintering, Biomaterials 17 (1996) 1787–1790, https://doi.org/10.1016/0142-9612(95)00356-8.
[20] L. Vecbiskena, K.A. Gross, U. Riekstina, T.C.K. Yang, Crystallized nano-sized alpha-tricalcium phosphate from amorphous calcium phosphate: microstructure, cementation and cell response, Biomed. Mater. 10 (2015), https://doi.org/10.1088/1748-6041/10/2/025009.
[21] S. Somrani, C. Rey, M. Jemal, Thermal evolution of amorphous tricalcium phosphate, J. Mater. Chem. 13 (2003) 888–892.
[22] S. Boudin, A. Grandin, M.M. Borel, A. Leclaire, B. Raveau, Redetermination of the β-Ca2P2O7 structure, Acta Crystallogr. Sect. C Cryst. Struct. Commun. 49 (1993) 2062–2064, https://doi.org/10.1107/S0108270193005608.
[23] K. Sudarsanan, R.A. Young, Significant precision in crystal structural details: holly springs hydroxyapatite, Acta Crystallogr. B25 (1969) 1534–1543, https://doi.org/10.1107/S0567740869004298.
[24] N. Doebelin, R. Kleeberg, Profex: a graphical user interface for the Rietveld refinement program BGMN, J. Appl. Crystallogr. 48 (2015) 1573–1580, https://doi.org/10.1107/S1600576715014685.
[25] B.H. Toby, R factors in Rietveld analysis: how good is good enough? Powder Diffr. 21 (2006) 67–70.
[26] N. Doebelin, Y. Maazouz, R. Heuberger, M. Bohner, A.A. Armstrong, A.J. Wagoner Johnson, C. Wanner, A thermodynamic approach to surface modification of calcium phosphate implants by phosphate evaporation and condensation, J. Eur. Ceram. Soc. 40 (2020) 6095–6106.
[27] A. Brangule, K.A. Gross, P. Anton, Biomatlante, B. Cam, EincoBio, Fundaciocim, himed, Subtilis, Effect on drying conditions on amorphous calcium phosphate, in: 26th Symp. Annu. Meet. Int. Soc. Ceram. Med. ISCM 2014, vol. 631, 2015, pp. 99–103, 10.4028Avww.scientific.net.KEM.631.99.
[28] L. Degli Esposti, S. Markovic, N. Ignjatovic, S. Panseri, M. Montesi, A. Adamiano, M. Fosca, J.V. Rau, V. Uskoković, M. Iafisco, Thermal crystallization of amorphous calcium phosphate combined with citrate and fluoride doping: a novel route to produce hydroxyapatite bioceramics, J. Mater. Chem. B 9 (2021) 4832–4845, https://doi.org/10.1039/D1TB00601K.
[29] F. Wakai, Modeling and simulation of elementary processes in ideal sintering, J. Am. Ceram. Soc. 89 (2006) 1471–1484, https://doi.org/10.1111/j.1551-2916.2006.01001.x.
[30] R. Raj, Analysis of the sintering pressure, J. Am. Ceram. Soc. 70 (1987) C-210–C–211, https://doi.org/10.1111/j.1151-2916.1987.tb05743.x.
[31] E. Ringdalen, Changes in quartz during heating and the possible effects on Si production, JOM (J. Occup. Med.) 67 (2015) 484–492, https://doi.org/10.1007/s11837-014-1149-y.
[32] M. Boudeulle, V. Joanny, P. Michel, Reviews in mineral phase transformations: some aspects of the eighties, Phase Transitions 32 (1991) 157–187, https://doi.org/10.1080/01411599108219174.
[33] P. Bouvier, E. Djurado, G. Lucazeau, T. Le Bihan, High-pressure structural evolution of undoped tetragonal nanocrystalline zirconia, Phys. Rev. B Condens. Matter 62 (2000) 8731–8737, https://doi.org/10.1103/PhysRevB.62.8731.
[34] A. Opalinska, I. Malka, W. Dzwolak, T. Chudoba, A. Presz, W. Lojkowski, Size-dependent density of zirconia nanoparticles, Beilstein J. Nanotechnol. (2015), https://doi.org/10.3762/bjnano.6.4.
[35] H. Monma, M. Goto, Behavior of the a-b Phase transformation in tricalcium phosphate, Yogyo-Kyokai-Shi 91 (10) (1983) 473–475.